Geophysical Research Letters

Supporting Information for

Limits to future expansion of surface-melt-enhanced ice flow into the interior of western Greenland

Kristin Poinar[1], Ian Joughin[1], Sarah B. Das[2],
Mark D. Behn[2], Jan T. M. Lenaerts[3], and Michiel R. van den Broeke[3]

[1]*Polar Science Center, Applied Physics Lab, University of Washington, Seattle, USA*
[2]*Dept. of Marine Geology and Geophysics, Woods Hole Oceanographic Inst., Woods Hole, MA, USA*
[3]*Institute for Marine and Atmospheric Research, Utrecht University, Utrecht, Netherlands*

Corresponding author: K. Poinar, `kpoinar@apl.washington.edu`

Contents of this file

Supplementary Text

Methods

We use four remotely sensed datasets to examine the observed and expected behavior of supraglacial lakes with elevation in western Greenland. We use satellite imagery from Landsat and RADARSAT to identify the current spatial distribution of supraglacial lakes, moulins, and streams in a 420,000-km^2 study area (the size of Sweden) in western Greenland. We also analyze surface-velocity-derived strain rates (Joughin et al., 2010) as a function of surface elevation (Howat et al., 2014; Joughin et al., 2010). The study area runs from approximately 63.0°N (south of Sermilik Glacier; -3000 km polar stereographic) to 70.5°N (north of Swiss Camp; -2000 km polar stereographic), and from the west coast inland to the divide. It is shown in Figure 1 of the main paper.

Model for the thermal state of the bed

We use a two-dimensional thermal model for ice sheets to calculate the basal temperatures and consequent thermal state along 27 flowlines spanning our study area. The model is unique because it is thermal rather than thermo-mechanical: that is to say, it uses the present-day ice-sheet geometry as a rigid domain, rather than spinning up in a way chosen to best match the current ice sheet. We use surface and basal elevations from Bamber et al. (2013) smoothed with a 20-km window and present-day surface velocity (Joughin et al., 2010). The model is also constrained by a climate history from the Summit ice core (Cuffey and Clow, 1997) scaled to present-day climate parameters (Ettema et al., 2009). We use one of two geothermal flux maps for the basal boundary condition: Shapiro and Ritzwoller (2004), which is seismically derived, and Fox Maule et al. (2005), which is based on magnetic data. We use two different geothermal flux datasets because

basal temperature is highly sensitive to this parameter (Rogozhina et al., 2012), which is not well validated due to a paucity of direct measurements in boreholes.

The model solves the heat equation, including multi-phase (polythermal) ice physics based on MacAyeal (1997), in a series of one-dimensional vertical columns that are linked to one another along a present-day flowline. Twenty-seven independent flowlines are interpolated to fill the study area. The spatial resolution of this product is approximately 50 km north-south and 5 km east-west. This asymmetry is because we wish to detect, along each east-west flowline, the inland frozen-thawed basal boundary, which we do not expect to vary greatly in the latitudinal direction (between adjacent flowlines). Our thermal model does not include surface-sourced water at the bed; that is, our basal heat sources are exclusively deformational, frictional, and geothermal.

Comparison of our model results with those of Seroussi et al. (2013) shows that they find a considerably larger area with a frozen bed. This likely results from refinements that Seroussi et al. (2013) made to the geothermal flux map to reflect the low heating rates observed at the bottom of the Dye-3 borehole. In particular, their model predicts a small, mid-elevation area with a frozen bed in the southern portion of our study region, at approximately y = -2800 km (Figure 1c). This area lies directly underneath freezing lakes and is therefore vulnerable, in theory, to the incursion of latent heat from surface meltwater. (The ice here has a surface elevation of approximately 1600–1800 meters, however, so we assert that it is at low risk of hydrofracture.)

We also compare our model results to those of Aschwanden et al. (2012). They used a spatially constant geothermal flux of 50 mW/m^2, which is somewhat lower than the average values in our study area given by Shapiro and Ritzwoller (2004) and Fox Maule et al. (2005). However, they find a wet bed extending inland to approximately the 2200-meter contour in the southern portion of our study area, and increasingly farther inland with latitude, to the 3000-meter contour in the northernmost portions of our study area.

They also find a mid-elevation frozen-bed area near the southern border of our study area, similar to but north of that detected by Seroussi et al. (2013). The frozen-bedded area of Aschwanden et al. (2012) spans approximately 400 kilometers and encompasses roughly 1800–2200 meters; many frozen-over lakes overly this area. If the bed is in fact frozen here, this area would be vulnerable to occasional basal speedup in the coming decades. For example, in the 2012 extreme melt year, Doyle et al. (2014) saw evidence of seasonalspeedup at 1840 meters elevation in this area of the ice sheet, although this speedup was likely caused by longitudinal coupling to lower-elevation regions where surface melt reached the bed.

A third modeling study (Rogozhina et al., 2012) did not detect any mid-elevation frozen-bedded areas. Because they used unadjusted geothermal flux from Shapiro and Ritzwoller (2004) and Fox Maule et al. (2005), this third study is most similar in nature to ours. They find a wet bet extending inland to approximately the 2400-meter contour.

In sum, because our model uses, in some places, a slightly higher geothermal flux than these previous studies, we consider our model results to be an upper bound on the melt extent. Our choice to use the 2000-meter contour as the approximate inland extent of a melted bed is conservative, as our results and the others discussed here find that the wet bed extends farther inland than that in most places within our study area.

Climatological analysis of the change in surface melt extent

We used RACMO2.3 output (updated from RACMO2.1 used by van Angelen et al. (2013)) of surface melt and surface mass balance (SMB) to study the changes in these quantities since 1958 in western Greenland. RACMO2.3 output is posted at 11 km. To study the changes in surface melt and SMB as a function of elevation, we resample the surface elevation (Howat et al., 2014) to this grid, then bin the melt and SMB model output into 100- and 200-meter elevation bands that span 0 to 3000 meters elevation. Higher elevation

bands (e.g., the 1900–2000 m band), which are wider (∼20 km), have more RACMO2.3 pixels than lower elevation bands (e.g., the 900–1000 m band), which can be as narrow as 3 km. To address this issue while still resolving the steep gradients in surface melt at lower elevations, we used 200-meter elevation bands at low elevations (surface elevations $s < 900$ m) and 100-meter bands at higher elevations ($s \geq 900$ m).

We test whether two populations of melt (or SMB) at each given elevation band are different at the 95% confidence level. Population 1 spans 1958–1987 (N_1 = 30 years) and Population 2 spans 1988–2013 (N_2 = 26 years). The test calculates the true mean of each population by considering the observed interannual variability over each period. We do not consider errors present in the RACMO output in this analysis.

For each elevation band, we run a two-tailed Student's t-test to determine the significance of the observed inland migration of melt (or the ELA). For this test, the t-statistic is given by

$$t = \frac{\bar{x}_1 - \bar{x}_2}{S_p \sqrt{1/N_1 + 1/N_2}},$$

$$\text{where } S_p = \sqrt{\frac{(N_1 - 1)s_1^2 + (N_2 - 1)s_2^2}{N_1 + N_2 - 2}},$$

where an overbar indicates the sample mean, N is sample size, s is sample standard deviation, and the subscripts 1 and 2 indicate each population (Devore, 1982). For 54 degrees of freedom (56 years minus the two means being calculated) in a two-tailed t-test, $t > 2.0049$ indicates that the two populations within a given elevation band are different at the 95% confidence level. Because each population contains measurements within 26 distinct elevation bands, we run this significance test 26 quasi-independent times. (The tests are not truly independent because of the coarseness of the melt model output, 11 km,

relative to the finer spacing, e.g. 3 km, in some lower elevation bands.) At 95% confidence, we would expect one or two bands to fail this test even if Populations 1 and 2 were truly different within those bands.

Our analysis of the surface melt model output shows that 23 of 26 elevation bands (88%) pass the t-test; the melt in these elevation bands has significantly changed since the earlier climatological period. (The RACMO 2.3 output in Figure 2 in the main paper shows that, at all elevations, this change is an increase.) The three bands that fail the t-test are s=200–400 m, 2600–2700 m, and 2700–2800 m; we cannot confidently say that melt has changed at these elevations. The low-elevation failed band (s=200–400 m) contained substantially fewer pixels than other bands (14 pixels compared to the average of 104 pixels) due to the steepness of terrain at low elevations, which may have caused it to fail. Furthermore, all three of these failed bands lie toward the ends of our tested elevations (0–3000 m). At the higher-elevation failed bands (2600–2800 m), our results indicate that surface melt may not be increasing; however, these elevations are substantially higher than both our identified upper limit of moulin formation ($\sim$1600 meters) and the frozen bed – wet bed transition ($\sim$2000 meters), so we do not analyze this further.

Our analysis of the SMB model output shows that only ten of the 26 elevation bands pass the t-test. In general, the elevation bands without a significant change in SMB span 1800–2800 meters elevation. In most elevation bands below 1800 meters elevation, which is roughly equivalent to the ELA (1630 meters averaged over the entire 56-year time period), there is a significant decrease in SMB. This suggests that the increased melt observed in the RACMO2.3 output at all elevations is, at high elevations, being at least partially offset by increased snowfall. Indeed, this is the expected behavior of an ice sheet in a warming climate (Cuffey and Paterson, 2010). Furthermore, the variation in SMB reflects changes in runoff rather than melt. Although melt is increasing at all elevations, increased melt rates also bring increased refreezing rates; thus, the change in runoff will

be less than the changes in melt, and overall, the change in SMB will be dampened compared to changes in surface melt. This may manifest in areas with little to no runoff: for example, the highest elevation bands studied (2800–3000 m). These bands showed a significant decrease in SMB between the two periods.

Inland migration distance of the ELA

Between the two periods of melt studied, the ELA rose 110 meters, from 1580 meters to 1690 meters. The average surface slopes in our study area at this elevation (Howat et al., 2014) indicate that this corresponds to an inland migration of 12 km. Because we are studying the average of two thirty-year periods, this migration distance represents the average migration over a thirty-year period. These distances differ from that found by Leeson et al. (2014), who studied the inland migration of the uppermost supraglacial lakes since 1971, i.e., over a 43-year period. Their result, 53 km, as well as that of Howat et al. (2013), 56 km over the same period, scale to 37 and 39 km over a thirty-year period, respectively. These distances are significantly longer than those revealed by our analysis of the ELA. However, when restricting the RACMO2.3 output to the smaller, more shallowly sloped study area of Leeson et al. (2014), we find an inland migration of the ELA of 38 km over the 30-year time period, which agrees well with the inland migration of the uppermost supraglacial lakes found by these two separate studies.

Identification of surface features

We used Landsat and radar images (from RADARSAT and ALOS-PALSAR) within our study area to identify surface streams and supraglacial lakes that do not drain completely by the end of each summer. Lakes with frozen lake ice lids visible in summertime Landsat imagery were identified as lakes that had formed the previous summer and overwintered

without draining (Darnell et al., 2013). Lake locations were confirmed with wintertime radar images, which highlight the contrast between lake ice caps and the surrounding ice sheet. We used images from 2000, 2010, and 2013 to identify frozen-over lakes because the greatest number of cloud-free Landsat images were available for these years. We use the presence of lake ice as the sole indicator that a lake overwintered without fully draining that year.

We used two visible-spectrum Landsat images (24 June 2004 and 30 July 2014) and radar images (an L-band ALOS-PALSAR mosaic from winter 2009-2010 as well as C-band RADARSAT mosaics from winters spanning 2000–2006) to identify and digitize the major surface streams in a smaller, centrally located area of approximately 6,000 km^2 (the size of Delaware). This region spans approximately 1100–1800 meters elevation (Figure 3a). We digitized a total of 312 major stream channels in this area. Though the width of the streams (approximately two meters or less) is less than the pixel size of the Landsat (30–70 meters) or radar (20 meters) data, the streams are nonetheless quite discernible; this is due to their long lengths ($\sim$10 km corresponds to $\sim$150–500 pixels), which allow the eye to identify adjacent pixels that are part of a linear feature. In most cases, the streams terminated into lakes or moulins that were conspicuous in the radar data as meter-scale bright spots, some of which were hundreds of meters downstream from lakebeds.

Visual inspection shows more complex surface water flow than we have digitized; Figure S1 illustrates the diversity of streams in the area over time (2004 and 2014) and space. While we digitized the major stream channels (red) from the 2004 image, the image clearly shows that these are fed by smaller, undigitized streams that we missed in 2004 (Figure S1a) and/or that intensified by 2014 (Figure S1d). Comparing the red digitized 2004 streams to the 2014 image they are overlain on also shows the slight migration of stream channels over time.

The lengths of these 312 streams tend to increase with elevation, as shown in Figure S2.

We find one long stream (35 km) originating at 1591 meters elevation; all other streams that originate at elevations <1600 meters (267 streams) are shorter than 30 km. By contrast, 70% (30 out of 44) of the streams originating above 1600 meters elevation are longer than 30 km. Stream length also becomes more variable with elevation, however: at 1200–1300 meters elevation, for example, the 39 identified streams are 6 $\pm$ 1 km long (95% confidence) on average, while at 1700–1800 meters elevation, the 15 identified streams average 40 $\pm$ 6 km in length. Despite the variability, this is a six-fold increase in stream length. Lower surface slopes likely play a role in the degree of stream lengthening. For example, surface slopes decrease by a factor of two to three, from 0.033 to 0.012, between 1200–1300 meters and 1700–1800 meters elevation in this area. This is markedly less than the factor-of-six increase in stream length observed for these same elevation bands, however. We therefore suggest that the absence of moulins at higher elevations is the primary explanation for the increased stream lengths there.

Strain rate dataset

We calculated the principal strain rate from wintertime velocity data averaged over 2007–2010 (Joughin et al., 2010). These data are posted at 500-meter resolution. We differenced these data to calculate the strain rates $\frac{\partial \vec{u}_i}{\partial \vec{r}_j}$, which therefore have 1-km resolution. We then used these strain rates to calculate the principal strain rate, following Cuffey and Paterson (2010):

$$\dot{\epsilon} = \frac{\partial u}{\partial x}\cos^2\theta + \frac{\partial v}{\partial y}\sin^2\theta,$$

$$\text{where } \theta = \frac{1}{2}\,\text{Tan}^{-1}\left(\frac{\dfrac{\partial u}{\partial y} + \dfrac{\partial v}{\partial x}}{\dfrac{\partial u}{\partial x} + \dfrac{\partial v}{\partial y}}\right)$$

These wintertime velocity data do not reflect higher summer velocities, which in land-terminating sectors of the ice sheet can be more than 50% greater due to meltwater-induced sliding enhancement (Joughin et al., 2008). Extensional strain rates thus reach their maximum in summer, when the differential seaward motion of the lower (below $\sim$1000 meters) and upper (above $\sim$1000 meters) parts of the ice sheet is at its peak. This is a direct result of surface meltwater reaching the bed. However, this effect lessens higher on the ice sheet: Palmer et al. (2011) observed only a 0.2% speedup at their station at 1716 meter elevation. At this elevation, the abundance of frozen-over lakes and the relative absence of moulins suggest that meltwater is not reaching the bed. Thus, we take wintertime data to be representative of summertime conditions higher on the ice sheet, where the implications of our study of strain rates are focused.

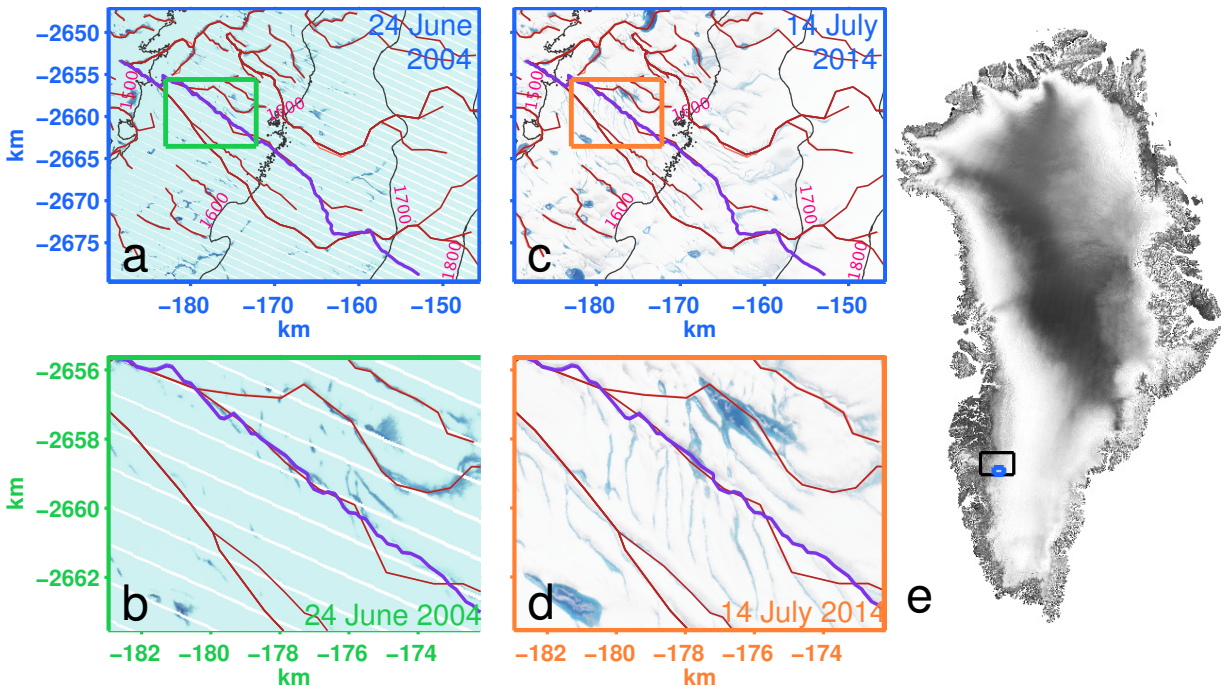

Figure S1

Landsat images (a–d) showing lakes and streams in southwestern Greenland. The black box in (e) indicates the location of Figure 4a in the main text, while the small blue box in (e) shows the location of panels (a) and (c) here (each sized 1400 km^2, the size of Rio de Janeiro). Panels (b) and (d) are 90-km^2 sub-areas of (a) and (c). The surface in June 2004 (a–b) and July 2014 (c–d) is shown, along with a subset of the 312 digitized streams (red) that span this area. Also shown is a long (∼47 km) surface stream that appears clearly in the 2014 imagery (purple diagonal line). Surface elevation contours from the GIMP DEM (Howat et al., 2014) are shown in black and labeled in pink. The black streams shown in Figure 4a were identified from the 2004 Landsat image shown here in panels (a–b) and updated with information from the 2014 Landsat image in panels (c–d).

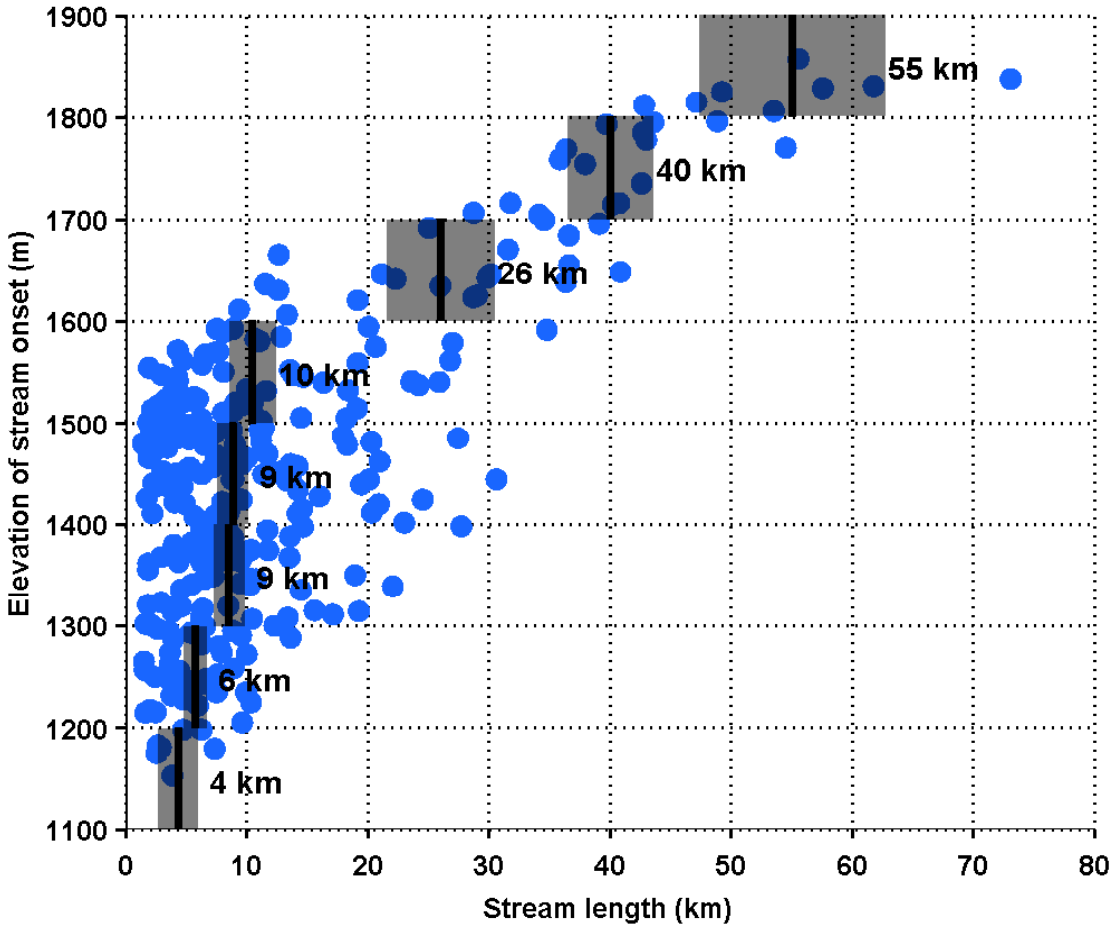

Figure S2

Stream length as a function of elevation, where the elevation of each stream is measured from the GIMP DEM (Howat et al., 2014) at the onset, or highest elevation, of the stream. Blue dots show the 312 streams we digitized; black lines show the mean stream length in each 100-meter elevation bin, with the 95% confidence interval shaded.

References

Aschwanden, A., E. Bueler, C. Khroulev, and H. Blatter (2012). An enthalpy formulation for glaciers and ice sheets. *Journal of Glaciology 58*(209), 441–457.

Bamber, J. L., J. A. Griggs, R. T. W. L. Hurkmans, J. A. Dowdeswell, S. P. Gogineni, I. Howat, J. Mouginot, J. Paden, S. Palmer, E. Rignot, and D. Steinhage (2013). A new bed elevation dataset for Greenland. *The Cryosphere 7*(2), 499–510.

Cuffey, K. M. and G. D. Clow (1997). Temperature, accumulation, and ice sheet elevation in central Greenland through the last deglacial transition. *Journal of Geophysical Research 102*(C12), 26383–26–396.

Cuffey, K. M. and W. S. B. Paterson (2010). The Physics of Glaciers.

Darnell, K. N., J. M. Amundson, L. M. Cathles, and D. R. MacAyeal (2013, July). The morphology of supraglacial lake ogives. *Journal of Glaciology 59*(215), 533–544.

Devore, J. L. (1982). *Probability & Statistics for Engineering and the Sciences*. California Polytechnic State University: Brooks/Cole Publishing Company.

Doyle, S. H., A. Hubbard, and A. Fitzpatrick (2014). Persistent flow acceleration within the interior of the Greenland ice sheet. *Geophysical Research Letters*.

Ettema, J., M. R. van den Broeke, E. van Meijgaard, W. J. van de Berg, J. L. Bamber, J. E. Box, and R. C. Bales (2009, June). Higher surface mass balance of the Greenland ice sheet revealed by high-resolution climate modeling. *Geophysical Research Letters 36*(12), L12501.

Fox Maule, C., M. E. Purucker, N. Olsen, and K. Mosegaard (2005, July). Heat flux anomalies in Antarctica revealed by satellite magnetic data. *Science 309*(5733), 464–467.

Howat, I. M., S. de la Peña, J. H. van Angelen, J. T. M. Lenaerts, and M. R. van den Broeke (2013). Expansion of meltwater lakes on the Greenland Ice Sheet. *The Cryosphere 7*(1), 201–204.

Howat, I. M., A. Negrete, and B. E. Smith (2014). The Greenland Ice Mapping Project (GIMP) land classification and surface elevation data sets. *Cryosphere 8*(4), 1509–1518.

Joughin, I., I. M. Howat, M. Fahnestock, B. Smith, W. Krabill, R. B. Alley, H. Stern, and M. Truffer (2008, October). Continued evolution of Jakobshavn Isbrae following its rapid speedup. *Journal of Geophysical Research 113*(F4), F04006.

Joughin, I., B. E. Smith, I. M. Howat, T. Scambos, and T. Moon (2010). Greenland flow variability from ice-sheet-wide velocity mapping. *Journal of Glaciology 56*(197), 415–430.

Leeson, A. A., A. Shepherd, K. Briggs, I. Howat, X. Fettweis, M. Morlighem, and E. Rignot (2014, December). Supraglacial lakes on the Greenland ice sheet advance inland under warming climate. *Nature Climate Change 5*(1), 51–55.

MacAyeal, D. R. (1997). EISMINT: Lessons in ice-sheet modeling. Technical report.

Palmer, S., A. Shepherd, P. Nienow, and I. Joughin (2011, February). Seasonal speedup of the Greenland Ice Sheet linked to routing of surface water. *Earth and Planetary Science Letters 302*(3-4), 423–428.

Rogozhina, I., J. M. Hagedoorn, Z. Martinec, K. Fleming, O. Soucek, R. Greve, and M. Thomas (2012, May). Effects of uncertainties in the geothermal heat flux distribution on the Greenland Ice Sheet: An assessment of existing heat flow models. *Journal of Geophysical Research 117*(F2), F02025.

Seroussi, H., M. Morlighem, E. Rignot, and A. Khazendar (2013). Dependence of century-scale projections of the Greenland ice sheet on its thermal regime. *Journal of Glaciology*.

Shapiro, N. M. and M. H. Ritzwoller (2004). Inferring surface heat flux distributions guided by a global seismic model: particular application to Antarctica. *Earth and Planetary Science Letters*.

van Angelen, J. H., M. R. van den Broeke, B. Wouters, and J. T. M. Lenaerts (2013, November). Contemporary (1960–2012) Evolution of the Climate and Surface Mass Balance of the Greenland Ice Sheet. *Surveys in Geophysics 35*(5), 1155–1174.